Heterogeneity of plastic flow of bimetals electrolytically saturated with hydrogen

Yulia Li, Svetlana Barannikova, Anna Bochkareva, Alexey Lunev, Galina Shlyakhova, and Lev Zuev

Citation: AIP Conference Proceedings **1783**, 020133 (2016); doi: 10.1063/1.4966426

View online: http://dx.doi.org/10.1063/1.4966426

View Table of Contents: http://scitation.aip.org/content/aip/proceeding/aipcp/1783?ver=pdfcov

Published by the AIP Publishing

Heterogeneity of Plastic Flow of Bimetals Electrolytically Saturated with Hydrogen

Yulia Li[1,2,a)], Svetlana Barannikova[1,2,3,b)], Anna Bochkareva[1,4,c)], Alexey Lunev[1,4,d)], Galina Shlyakhova[5,e)], and Lev Zuev[1,2,f)]

[1] *Institute of Strength Physics and Materials Science SB RAS, Tomsk, 634055 Russia*
[2] *National Research Tomsk State University, Tomsk, 634050 Russia*
[3] *Tomsk State University of Architecture and Building, Tomsk, 634003 Russia*
[4] *National Research Tomsk Polytechnic University, Tomsk, 634050 Russia*
[5] *Seversk State Technological Institute (National Research Nuclear University MEPhI), Seversk, 636036 Russia*

[a)] Corresponding author: jul2207@mail.ru
[b)] bsa@ispms.tsc.ru
[c)] avb@ispms.tsc.ru
[d)] agl@ispms.tsc.ru
[e)] shgv@ispms.tsc.ru
[f)] lbz@ispms.tsc.ru

Abstract. This paper presents the study of a corrosion-resistant bimetal composed of austenitic stainless steel (301 AISI) and low-carbon construction steel (A 283 Grade C) and the effect of its electrolytic hydrogenation on plastic flow of the test material. Localization patterns of plastic deformation in the process of uniaxial tension were obtained using the digital image correlation method. The evolution of localized plastic deformation zones was studied in the initial state and after electrolytic hydrogenation. The staging of stress-strain curves was analyzed.

INTRODUCTION

Currently, regularities of plastic deformation at micro-, meso- and macroscopic scales are identified and studied for a wide range of pure metals or alloys [1–5]. Localizations of plastic deformation at the macroscopic scale of different forms can be considered as different types of autowaves that depend on the strain hardening law taking place at this stage [4, 5].

A limited number of studies are devoted to deformation behaviors of multilayer materials exposed to intensive plastic deformation. Such materials can be composed of various metals joined together in monoliths that retain a reliable binding between the components under further technological treatment and in operation. These materials include two-layer metal composites—bimetals, in particular anti-corrosion bimetals that are highly resistant to aggressive media and have high mechanical characteristics [6–9]. Compositions of carbon and corrosion-resistant steels in the form of thin and thick sheets, as well as in the form of pipes account for the largest share in the production of corrosion-resistant bimetals in chemical, oil-refining, pulp and paper, food and ship-building industries.

This paper is aimed at studying patterns of plastic deformation and fracture of a bimetal composition of carbon steel and high-chromium stainless steel exposed to uniaxial tension in an aggressive hydrogen-containing medium. When penetrating into structural elements and details, a hydrogen-containing medium causes considerable deterioration of short- and long-term mechanical properties of a material. This leads to a change of stress-strain behavior and a significant decrease in bearing capacity and strength of structures [10–13].

Advanced Materials with Hierarchical Structure for New Technologies and Reliable Structures 2016
AIP Conf. Proc. 1783, 020133-1–020133-4; doi: 10.1063/1.4966426
Published by AIP Publishing. 978-0-7354-1445-7/$30.00

RESEARCH MATERIALS AND METHODS

In this work, anti-corrosion bimetal that consists of the austenitic stainless steel (301 AISI) and low-carbon steel (A 283 Grade C) is considered. This bimetal was produced via pouring followed by rolling to the required thickness of 8 mm. The thickness of the cladding layer was 0.6 mm. For the purpose of this study, test samples were produced from the bimetal in the shape of dog bones with the gage section measuring 40×8×2 mm.

Electrolytic hydrogenation of the bimetal samples was carried on during 6h under the controlled cathode potential of –600 mV relative to the reference electrode of silver chloride in the 1N solution of sulphuric acid with an addition of 20 mg/L of thiourea [14]. Mechanical tests were carried out at the rate of 6.67×10^{-5} s^{-1} at room temperature in a universal testing machine LFM-125. A detailed study of plastic yielding localization patterns at the macroscopic scale was performed using a ALMEC-tv universal measuring system for digital recording of displacement vector fields and a tensor component of plastic distortion [15].

EXPERIMENTAL RESULTS

A microstructural analysis showed that a carbonized zone was formed in the interface in the austenitic stainless steel, while a heavily decarbonized zone with a ferrite structure was generated in the low-carbon construction steel. The transition area was studied in detail by scanning electron microscopy using CARL ZEISS EVO 50 and an energy dispersive spectroscopy software from Oxford Instruments (NANOTECH Shared Use Center of ISPMS SB RAS). The study showed that the A 283 Grade C steel exhibited traces of chromium carbide when approaching the interface. The chromium content increased from 0.18 to 0.39 wt % at the depth of 25–5 μm from the interface, which was conditioned by chrome diffusion from the stainless steel into the A 283 Grade C steel (Fig. 1a, Table 1).

Figures 1b and 1c present the analysis of trace components for the stainless steel: it is shown that the carbon content increases from 2.08 wt % on the surface to 2.75 wt % at 10 μm to the interface of 301 AISI stainless steel (see Table 1). At the same distance and less than 10 μm from the interface, carbides are generated due to diffusion of alloying elements from the 301 steel into the A 283 Grade C steel on the boundary of the compound.

As a result of mechanical testing, stress-strain curves of the bimetal in the initial state (*1*) and after 6-hour hydrogenation (*2*) were obtained (Fig. 2).

The stress-strain curve can be related to diagrams of the general type. Therefore, it can be described by the Lüdwick equation (1)

$$\sigma = \sigma_0 + K\varepsilon^n, \tag{1}$$

where K is a work-hardening coefficient, $n \le 1$ is a work-hardening index.

Analysis of the stress-strain curves in states *1* and *2* using the method described in [8] revealed the following stages of plastic flow: yield drop and plateau forming [7], linear work hardening, parabolic work hardening, and prefracture. As a result of 6-hour electrolytic hydrogenation, strength of the bimetal decreased slightly, while its plasticity increased.

Digital image correlation was used to study the evolution of plastic deformation localization patterns in the cladding layer of 301 AISI stainless steel, the bonding layer of A 283 Grade C low-carbon steel and the transition layer of the material at all work hardening stages for states *1* and *2*.

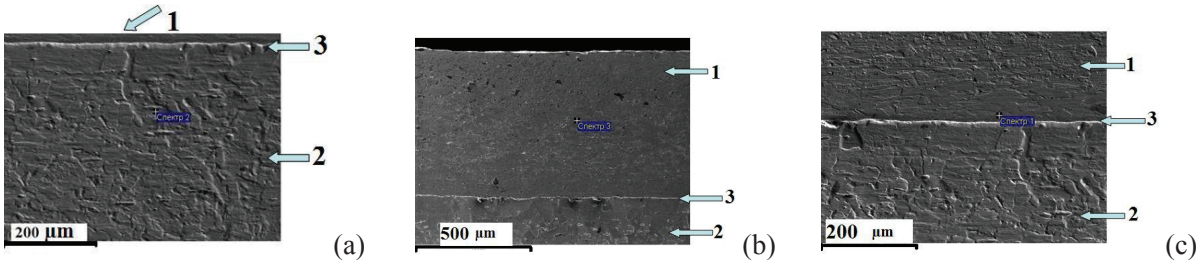

FIGURE 1. SEM image of the bimetal (*1*—301 AISI, *2*—A 283 Grade C, *3*—interface) at different distance to the transition area: (a) 150 μm to the interface, (b) 315 μm to the interface, (c) 8 μm to the interface

TABLE 1. Dispersive X-ray microanalysis of the bimetal in Fig. 1

Distance to the transition area, μm	Element						
	C, wt %	Si, wt %	Ti, wt %	Cr, wt %	Mn, wt %	Fe, wt %	Ni, wt %
A 283 Grade C							
150	–	0.19	–	–	0.59	99.22	–
25	–	0.20	–	0.18	0.56	97.07	–
5	–	0.25	–	0.39	0.51	98.90	–-
301 AISI							
315	2.08	0.45	0.26	16.14	1.00	69.27	10.80
8	2.75	0.40	0.19	15.5	1.14	69.69	10.35

As shown by the analysis of plastic deformation localization patterns of the bimetal in states *1* and *2*, the primary system of movable localized plastic deformation areas is generated on the yield line in the cladding and transition layers of the material. Later in the process of deformation, individual fronts become separated from them in the area of the interface bonding layer at the depth of 0.7 mm and continue their coordinated movement along the axis of tension but at other velocities than the localized deformation areas of the stainless steel layer.

In addition to the above-described pattern, four equidistant movable localized plastic deformation areas are formed in the area of the base material (A 283 Grade C steel) at the linear work-hardening stage for states *1* and *2*. However, movable areas in 301 AISI stainless steel and plastic deformation areas in the transition area of the material prevent them from propagating at a constant speed along the length of the sample.

At the parabolic work-hardening stage at the general deformation ε = 12% for state *1* and at ε = 13% for state *2*, stationary systems of equidistant localized plastic deformation areas are formed.

At the prefracture stage in state *1* and *2*, localized plastic deformation areas that have been immobile show a tendency to confluence and start their coordinated movement to the high-amplitude peak of local deformations formed in the fractured portion of the sample (Fig. 3).

Fractures of the material in states *1* and *2* are of a different nature. The fracture in state *2* is more ductile. Two macroscale bands of localized plastic deformation are formed in the initial state *1* in the area of a macroscopic stress concentrator at the necking stage at the general deformation ε = 32.6%. They propagate towards the maximum tangential stresses and give a rise to the main crack. The main crack is generated in the area of the bimetal protective layer and quickly propagates throughout the section of the sample.

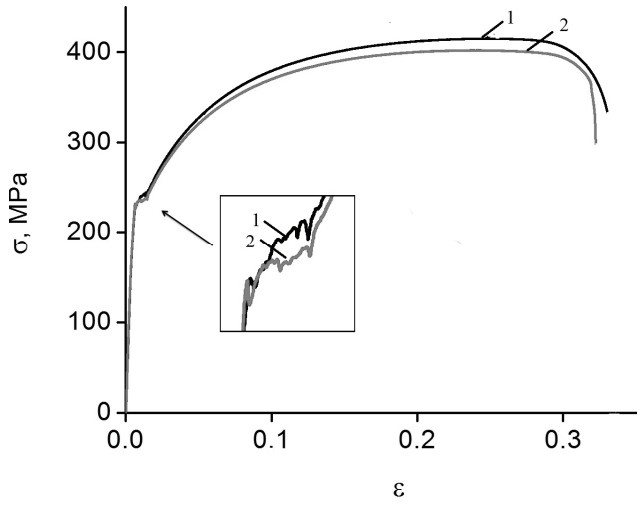

FIGURE 2. Diagram of bimetal loading in the initial state (*1*) and after 6-hour electrolytic hydrogenation (*2*)

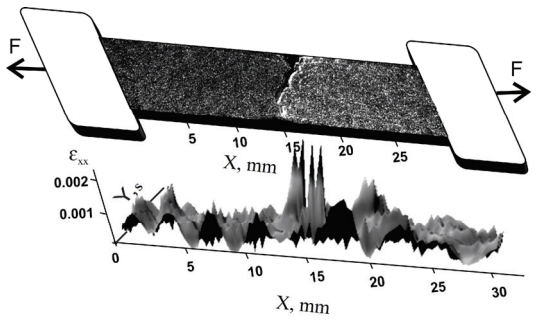

FIGURE 3. Bimetal fracture patterns and distribution of local extensions at the pre-fracture stage

One macroscale band of localized plastic deformation is formed in state *2* after electrolytic hydrogenation of the bimetal at the general deformation ε = 31.7%. Breakage resistance is found to improve as compared to state *1*. During the movement, the main crack is divided into a series of separate small cracks that reduce the propagation velocity of the main crack and improve fracture toughness of the material. The main crack is of a zigzag shape and propagates brokenly. While moving, it changes its position and direction of propagation. It should be noted that the crack path is conditioned by the position of localized plastic deformation areas at early plastic yielding stages that are indicative of future fracture.

CONCLUSIONS

This study has found that localized plastic deformation areas are formed and evolve during tension of 301 bimetal samples both in the initial state *1* and after 6-hour electrolytic hydrogenation throughout plastic yielding in primary, protective and transitional layers of the bimetal. It has been established that in the initial state *1* a decarbonized layer is formed in the bimetal on the side of A 283 Grade C steel, while a carbonized layer is formed on the side of 301 AISI steel. Moreover, an intermediate layer (carbide) of up to 50 μm depth has been found at the boundary. The bimetal fracture process in states *1* and *2* is caused by stress concentration in the bimetal transition layer. Origination and propagation of a crack can be localized at early work-hardening stages. The fracture of the samples after hydrogenation is more ductile as compared with the primary material, which is indicative of the fact that in this case hydrogen atoms increase plasticity of the austenitic stainless steel layer of the test bimetal.

ACKNOWLEDGMENTS

The work was performed in the framework of the Program of Fundamental Research of State Academies of Sciences for the period 2013–2020 and supported in part by the Russian Foundation for Basic Research (project No. 16-38-50234 mol_nr).

REFERENCES

1. R. N. Mudrock, M. A. Lebyodkin, P. Kurath, A. Beaudoin, and T. A. Lebedkina, Scripta Mater. **65**, 1093–1095 (2011).
2. T. V. Tretiakova and V. E. Vildeman, Fratt. Integ. Struct. **24**, 1–6 (2013).
3. S. A. Barannikova, Tech. Phys. **45**, 1368–1370 (2000).
4. L. B. Zuev and S. A. Barannikova, Int. J. Mech. Sci. **88**, 1–7 (2014).
5. S. A. Barannikova, Tech. Phys. Lett. **30**, 338–340 (2004).
6. H. E. M. Sallam, Kh. Abd El-Aziz, H. Abd El-Raouf, and E. M. Elbanna, Mater. Des. **52**, 974–980 (2013).
7. I. Chen, Z. Yang, B. Jhan, J. Xia, and J. W. Stevenson, J. Power Sources **152**, 40–45 (2005).
8. J. Y. Jin and S. I. Hong, Mater. Sci. Eng. A **596**, 1–8 (2014).
9. J. E. Lee, D. H. Bae, W. S Chung, K. H. Kim, J. H. Lee, and Y. R. Cho, J. Mater. Process. Technol. **187–188,** 546–549 (2007).
10. V. P. Ramunni, T. De Paiva Coelho, and P. E. V. de Miranda, Mater. Sci. Eng. A **435–436**, 504–514 (2006).
11. P. Sofronis, Y. Liang, and N. Aravas, Eur. J. Mech. A: Solids **20**, 857–872 (2001).
12. I. M. Robertson, Eng. Fract. Mech. **68**, 671–692 (2001).
13. Y. Yagodzinskyy, T. Saukkonen, S. Kilpeläinen, F. Tuomisto, and H. Hänninen, Scripta Mater. **62**, 155–158 (2010).
14. L. B. Zuev, S .A. Barannikova, M. V. Nadezhkin, and V. A. Mel'nichuk, Tech. Phys. Lett. **37**, 793–796 (2011).
15. L. B. Zuev, V. V. Gorbatenko, and K. V. Pavlichev, Measur. Sci. Technol. **21**, 1–5 (2010).